Heterogeneous C–H Functionalization in Water *via* Porous Covalent Organic Framework Nano Films: A Case of Catalytic Sphere Transmutation

Rahul Banerjee (r.banerjee@ncl.res.in)
Indian Institute of Science Education and Research
Himadri Sasmal
Indian Institute of Science Education and Research Kolkata
Saikat Bag
Indian Institute of Science Education and Research
Bittu Chandra
Indian Institute of Science Education and Research
Poulami Majumder
Indian Institute of Science Education and Research
Himangshu Kuiry
Indian Institute of Science Education and Research
Sayam Sengupta
Indian Institute of Science Education and Research

Article

Keywords: crystal engineering, covalent organic framework (COF) nano-spheres

Posted Date: January 22nd, 2021

DOI: https://doi.org/10.21203/rs.3.rs-142407/v1

Abstract

Heterogeneous catalysis in water has not been explored beyond certain advantages like recyclability and recovery of the catalysts from the reaction medium. In doing so, they often fail to address other authentic pitfalls of homogeneous catalysis. Moreover, poor yield, extremely low selectivity, and active catalytic sites' deactivation further underrate the heterogeneous catalysis in water. On the other hand, most of the synthetically useful homogeneous catalysts are either water intolerant or remain catalytically inactive in water. Considering these facts, we have rationally designed and synthesized solution dispersible porous covalent organic framework (COF) nano-spheres to utilize their distinctive morphology and dispersibility to bridge between homogeneous and heterogeneous catalysis. The success has further been extended in fabricating catalyst immobilized COF thin-films *via* covalent self-assembly for the very first time. We have used these catalyst immobilized COF thin-films to develop a general methodology for the C-H functionalization of organic substrates in water. This unique covalent self-assembly occurs through the protrusion of the fibers/threads at the interface of two nano-spheres, transmuting the catalytic spheres into films without any leaching of catalyst molecules, which was hitherto unheard of. The catalyst immobilized porous COF thin-films' chemical functionality and hydrophobic environment stabilizes the high valent transient active oxoiron(V) intermediate in water and restricts the active catalytic site's deactivation. An elevated catalytic yield and high selectivity (3°:2°) have been achieved in open-air conditions at room temperature, accompanying the elemental feature of heterogeneous catalysis, i.e., the recyclability. These COF films functionalized the unactivated C-H bonds in water with a high catalytic yield (45-99%) and with a high degree of selectivity (*cis:trans*=155:1; 3°:2°=257:1 in case of *cis*-1,2-dimethylcyclohexane). To establish the "practical implementation" of this approach, we conducted the inflow catalysis (Turnover Number = 355±5) using catalyst immobilized COF films fabricated on a macroporous polymeric support.

Introduction

Direct and selective functionalization of inert C-H bonds as a latent functional group in water is a demanding endeavour,[1-5] although enzymes do the same transformation under ambient conditions.[6-8] However, most enzymes are expensive and lose their catalytic activity with a slight alteration of reaction conditions.[9] A few homogeneous catalysts and catalytic methods have already been developed to functionalize inert C-H bonds in water.[10-14] For example, μ-nitrido diiron phthalocyanine and porphyrin complexes were found to catalyze the oxidation of CH_4 in water.[15] However, selective oxidative functionalization of complex molecules, analogous to the chemical processes that occur in all living systems, with appreciable catalytic activity and selectivity in water, is exceptionally challenging. Water is economical and green, and pharmaceutical and biologically relevant molecules are generally only soluble in water/polar media.[16-17] Hence, a challenging new area of catalysis research should be to develop a general protocol where most of the catalytic processes are performed in water. However, many

synthetically useful catalysts will get excluded in such cases because of their loss of catalytic activity or intolerance towards the water. Additionally, most organic substrates are insoluble in water. A pragmatic solution to this problem would be to use ordered organic hydrophobic porous supports that could entrap both the catalyst and substrate in close proximity to significantly enhance the reaction rate. This concept of integrating one or more catalytically active functionalities and substrates into a solid organic host material would mimic enzymes such as cytochrome P450, in which the hydrophobic active site holds both the heme cofactor and the substrate in close proximity. Whereas this strategy seems easy, it poses problems because of the challenges associated with designing such crystalline yet hydrophobic and porous organic host structures.

We envisaged that catalyst encapsulation within a chemically stable porous covalent organic framework (COF) could be a strategy to provide a hydrophobic microenvironment around the active site so that the catalytic process could be performed in the aqueous media. Covalent organic frameworks (COFs) are a new class of crystalline materials, with highly ordered organic building blocks and discrete nano-pores.[18-22] The organic building units in COFs, stacked into infinite 1D columns, are ideal for docking catalysts and providing a hydrophobic microenvironment around the active site.[23-25] Hence, we designed a nano-spherical formulation of a two-dimensional covalent organic framework with predesigned functionality. These nano-spheres can be used to immobilize catalysts *via* non-covalent interactions. Simultaneously, the material's porous nature would allow free diffusion of the substrate and the products formed after the reaction.

The first catalyst that was immobilized is a member of the fifth-generation biuret modified TAML, $(Et_4N)_2[Fe^{III}(Cl)bTAML]$, which catalyzes the selective hydroxylation of C–H bonds with very high regioselectivity (3° C–H over 2° C–H) and stereoretention.[26,27] This bioinspired catalyst typically activates oxo transfer reagents, such as *m*CPBA, NaOCl, or O_2, to oxidize alkane bonds and alkenes to their corresponding oxidized products. Herein, we present a unique strategy for concerted heterogeneous catalysis by generating a catalytically active FebTAML complex within the inter-crystallite voids of the COF nano-spheres. Furthermore, noting the FebTAML immobilized COF nano-spheres' inability to functionalize C–H bonds in water, we decided to transmute the catalyst loaded COF nano-spheres into thin-films. We could fabricate such self-standing COF thin-films, as these crystalline and porous COF nano-spheres[28] undergo mesoscale "fiber protrusion". We took advantage of this exceptional phenomenon to arrest $(Et_4N)_2[Fe^{III}(Cl)bTAML]$ molecules during the nano-spheres ® thin-film transmutation. It is fascinating that the immobilized catalyst molecules remained entrapped despite such dynamic transmutation and culminated into highly fecund catalytic COF thin-films. To the best of our knowledge, this is the first example of the selective C–H functionalization of the water-insoluble hydrophobic substrates in pure water using the catalyst immobilized self-standing thin-films. We believe that the organic substrates preferentially partitioned inside the COF film, allowing water-insoluble substrate oxidation in water. Finally, we performed inflow catalysis using catalyst immobilized COF thin-films on a macroporous solid polymeric support. After the 60^{th} cycle, this inflow catalysis showcased the efficacy of the system, with 72% catalytic yield and an excellent [~355] turnover number.

Results And Discussion

The TpDPP COF nano-spheres were synthesized by the reaction between the 0.03 mmol triformylphloroglucinol (Tp), and 0.045 mmol 3,8-diamino-6-phenylphenathridine (DPP) in the presence of a catalytic amount (10-15mL) of trifluoroacetic acid (figure 1a and section S-2). The reaction conditions first led to the direct nucleation of the organic building blocks, followed by spatiotemporal growth. The formation of the organic framework structure of the COF nano-spheres could be ascertained by the intense PXRD peak at [3.65±0.06] (2θ) imputed to their (100) plane diffractions (Figure 1d).[29] The experimental diffraction pattern manifests good agreement with the slipped-AA stacking models¢ simulated powder diffraction pattern. Additionally, the Pawley refinement between the simulated slipped-AA model and the experimental powder diffraction pattern using the Reflex Plus module of the Material Studio (Figure S2) showed good agreement (R_p = 4.5%, R_{wp} = 5.4%). The N_2 adsorption analysis revealed a surface area (S_{BET}) of 686 m^2g^{-1} with a uniform pore size (~1.9 nm) distribution (Figure S8 and S9). The FTIR spectra of TpDPP nano-spheres displayed intense peaks at 1600–1625 (–C=O), 1579 (–C=C), 1277 cm^{-1} (–C–N), and peaks at 1671 (–C=O of free –CHO), 2851-2920 (–C–H of free –CHO), 3067-3352 cm^{-1} (–N–H stretching of free $–NH_2$) (Figure S5). The FTIR spectra suggested the formation of a β-ketoenamine backbone[30-32] and the presence of free aldehyde and amine functionalities on the sphere surface. The presence of free aldehyde and amine functionalities indicates incomplete crystallization and structural defects. The zeta potential of the colloidal COF nano-spheres in DCM was measured to be +65.4 mV at 20 °C, which suggests the presence of the defused positive charges at the interface between the solid COF nano-spheres and the solvent molecules (Figure 2e). As expected, the dispersible COF nano-spheres' zeta potential dropped to +9.5 mV after neutralization with triethylamine (Et_3N) (Figure 2f). The dynamic light scattering (DLS) analyses revealed the as-synthesized COF nano-spheres¢ average size to be in the range of 590-610 nm (Figure 2e-f). The size and zeta potential of COF nano-spheres remained unaltered (626 nm and +65.4 mV as-synthesized vs. 632 nm and +61.7 mV) for four months (Figure 2g and 2j). Such a constant presence of permanent positive charges at the solid-liquid interface made these nano-spheres stable in solution and prevented their aggregation.

The high surface area and defects within the COF nano-spheres made them a promising candidate for the physisorption of catalytically active $(Et_4N)_2[Fe^{III}(Cl)bTAML]$ molecules within the condensed space. In enzyme catalysis, the amide functionalities of the enzyme backbone or the charged amino acid side chains can influence the active sites' electronic properties through long-range interactions.[33] We envisaged that the hydrogen bonding between the first coordination sphere amide functionality (–C=O) of the $(Et_4N)_2[Fe^{III}(Cl)bTAML]$ molecules and the free $–NH_2$ of the COF nano-spheres has a significant effect on the catalytic reactivity and selectivity. Such increased reactivity towards oxidation reactions upon binding Lewis acids to the ligand carbonyl in the related oxo Mn(V)-TAML complexes has been reported earlier.[34,35] The Raman spectra of the $(Et_4N)_2[Fe^{III}(Cl)bTAML]$ catalyst obtained upon 785 nm excitation revealed the presence of an Am I (–C=O stretch) band at 1616 cm^{-1} and an Am II (C–N stretch) band at 1569 cm^{-1}. The catalyst Am I (–C=O stretch) band red-shifted to 1601 cm^{-1}, and a new peak appeared at

1621 cm^{-1} due to the immobilization of the catalyst inside the COF nano-spheres. Similarly, the catalyst Am II (C–N stretch) band blue-shifted to 1573 cm^{-1}, and a new peak appeared at 1562 cm^{-1} (Figure S31). This shift in –C=O and C–N stretch bands indicates the presence of N—H···O hydrogen bonding between the free amine of the COF nano-sphere and the amide carbonyl of the immobilized catalyst.[36,37] The XPS analysis of the $(Et_4N)_2[Fe^{III}(Cl)bTAML]$ catalyst revealed the deconvoluted C 1s spectra, which indicates the presence of two distinct peaks at 286.1 and 287.1 eV corresponding to the amide carbon and the diamide carbon, respectively (Figure S32-33). While immobilized inside the COF nano-sphere, these two peaks appeared at almost similar regions (286.6-286.9 eV) due to the hydrogen bonding and could not be appropriately resolved.[38]

1.0 mg of solid COF nano-spheres can immobilize ~95% $(Et_4N)_2[Fe^{III}(Cl)bTAML]$ catalyst from 1 ml 0.2 and 0.4 mM solution in acetonitrile (Figure S14-15). We believe that the positively charged COF nano-sphere matrix, containing $–NH_3^+$ and N–H functional groups, drives the immobilization of negatively charged $[Fe^{III}(Cl)bTAML]^{2-}$ molecules. Consequently, we can control the wt% loading of the immobilized catalyst within the dispersible COF nano-spheres by increasing the amount of COF nano-spheres and keeping the concentration of the catalytic solution (1 ml 0.4 mM solution in acetonitrile) constant (Figure S55 and section S-19). We deliberately formulated COF nano-spheres for catalyst immobilization because of their adsorption capacity, by considering a similar quantity of highly crystalline COF powder[39] and films (Figure S12). TpDPP COF powder (1565 m^2g^{-1}) and thin-film (1265 m^2g^{-1}) do have a higher surface area compared to the nano-spheres (686 m^2g^{-1}). However, the catalyst adsorption capacity of the COF nano-spheres (94.8%) is 2-3 times higher than the COF powder (47%) and COF thin-films (21%). Furthermore, the COF nano-spheres' ability to transmute into thin-films gave us another avenue to fabricate COF thin-films with a higher amount of immobilized catalyst. The dispersible COF nano-spheres achieved 90% of their absorption efficiency within 90 seconds. The maximum uptake of the $(Et_4N)_2[Fe^{III}(Cl)bTAML]$ catalyst by the as-synthesized TpDPP COF nano-spheres was found to be 378.9 mg g^{-1}. We have performed the identical absorption experiment with another iron-based electrophilic homogeneous catalyst $[Fe^{II}(S, S\text{-}PDP)](SbF_6)_2$, which is a cationic complex and also known to catalyze the hydroxylation reaction of C-H bonds (Figure S16-17). The immobilization of $[Fe^{II}(S,S\text{-}PDP)](SbF_6)_2$ into the porous COF nano-sphere matrix was only 36%, due to the ionic repulsion between the two cationic species.

In CH_3CN, $[Fe^{III}(Cl)bTAML]^{2-}$@1X TpDPP COF nano-spheres (catalyst immobilized from 1 ml 0.4 mM acetonitrile solution by 1 mg of COF nano-spheres) was found to catalyze the hydroxylation of adamantane (8 mM; 20 eq.) with NaOCl (0.1 M, 250 eq.) to yield 1-adamantol as the primary product with a 45:1 selectivity for the 3° C-H bond over the 2° C-H bond (Figure 3c). Optimization reactions performed with various $(Et_4N)_2[Fe^{III}(Cl)bTAML]$ loaded COF nano-spheres indicated that the maximum reactivity (73% conversion, 70% yield) and selectivity (3°:2º=101:1) was observed for $[Fe^{III}(Cl)bTAML]^{2-}$@2X TpDPP COF nano-spheres (catalyst immobilized from 1 ml0.4 mM acetonitrile solution by 2 mg of COF nano-

spheres) (Figure S55). This optimization study indicated that maximum loading of COF nano-spheres with $(Et_4N)_2[Fe^{III}(Cl)bTAML]$ reduced the selectivity of oxidation due to possible processes involving dimeric oxoiron intermediates formed due to their proximity. On the contrary, when the loading was significantly reduced, the conversions decreased, indicating that the rates slowed due to excess COF present. Based on this data, $[Fe^{III}(Cl)bTAML]^{2-}$@2X TpDPP COF nano-spheres were employed as the catalyst for all subsequent reactions. Control reactions

performed with only NaOCl (0.1 mM) or bare COF nano-spheres afforded <5% products. We have explored the oxidation of a series of substrates containing unactivated 3° C-H bonds and 2° benzylic C-H bonds using $[Fe^{III}(Cl)bTAML]^{2-}$@2X TpDPP COF nano-spheres as the catalyst and NaOCl as the oxidant in CH_3CN under the optimized conditions (Figure 3f and section S-19). The heterogeneous oxidation of adamantane, having twelve 2° C-H and four 3° C-H bonds afforded selectively 1-adamantanol in ~70% yield with remarkably high regioselectivity (i.e., 101:1) of the 3° C-H bond over the 2° C-H bond (Figure 3c). In the case of *cis*-1,2-dimethylcyclohexane, *trans*-1,2-dimethylcyclohexane, and *cis*-decalin (Figure 3f), mainly 3° hydroxylated products were obtained in 90%, 42%, and 85% yields with 99% stereo-retention. Substrates having activated benzylic C-H bonds such as ethylbenzene (EB), diphenylmethane (DPM), dihydroanthracene (DHA), and xanthene were explored. Primarily ketone products were formed for all these substrates with high conversion and yield (Fig. 3f-h). The oxidation of 3° C–H bonds in simple hydrocarbons was then extended to natural product derivatives. For example, cedryl acetate, a natural product derivative of cedrol found in essential oil, having a rigid structure with five 3° C–H bonds, affords a single hydroxylated product in 70% yield (Figure 3h). Ambroxide, a naturally occurring terpenoid used in perfumery, undergoes exclusive oxidation at the alpha ethereal C–H bond predominantly among many other electronically and sterically accessible secondary and tertiary C–H bonds (Figure 3h). Finally, the use of alkenes as substrates led to the corresponding epoxides' formation in high yields (60-99%) (Figure 3g). During these catalytic reactions, the products formed parallel those that have been found under homogeneous conditions using Fe-bTAML analogs and NaOCl. We have previously demonstrated[40] that $(Et_4N)_2[Fe^{III}(Cl)bTAML]$ reacts with NaOCl to form the active oxoiron(V) intermediate, which is responsible for substrate oxidation. For the $[Fe^{III}(Cl)bTAML]^{2-}$@2X TpDPP COF nano-spheres, X-band EPR spectrum at 123K (Figure S34) manifested a rhombic S= ½ species with g = 2.00, 1.93, and 1.73, which indicated that the same oxoiron(V) intermediate was generated inside the COF nano-spheres, which confirms that the overall mechanism of oxidation remained unchanged upon immobilization of the catalyst.

Although the overall mechanism of oxidation remains unchanged, several aspects are worth noting. The selectivity obtained for the oxidation of hydrocarbons in the $[Fe^{III}(Cl)bTAML]^{2-}$@COF nano-spheres far exceeds what is observed under homogeneous conditions. For catalytic oxidation of adamantane using $(Et_4N)_2[Fe^{III}(Cl)bTAML]$/NaOCl under homogeneous conditions in air, the selectivity towards 3º C-H is reduced nearly four-folds (110:1 in the absence of air to 31:1 in the presence of air). This reduction in selectivity occurs since some of the carbon-centered radicals formed during C-H abstraction react with O_2 *via* the "non-rebound" pathway leading to an additional free radical auto-oxidation pathway. In fact,

during the homogeneous oxidation of adamantane in air, 1-adamantanol is formed along with other products such as 2-adamantanol and 2-adamantanone (9-10%), which significantly reduces the regioselectivity of 3° C-H bond oxidation over 2° C-H bonds.

However, the regioselectivity obtained for adamantane oxidation by $[Fe^{III}(Cl)bTAML]^{2-}$@2X TpDPP COF nano-spheres, in the presence of O_2, is similar (3°:2° = 101:1 based on the statistical correction for the number of C–H bonds) to that obtained for reactions that were performed under homogeneous conditions with $(Et_4N)_2[Fe^{III}(Cl)bTAML]$ in the absence of O_2.[41,42] Such regioselectivity could be due to the total shutdown of the free-radical pathway since the hydrophobic scaffold of the COF nano-spheres creates an appropriate binding pocket for both the anionic macrocyclic catalyst (*via* ionic interactions) and the substrate (*via* predominantly hydrophobic interactions). Consequently, the carbon-centered radical formed upon C-H abstraction does not escape to the bulk to react with O_2, thereby initiating a free-radical process that would significantly reduce the selectivity. Therefore, the oxidation mechanism solely involves the "rebound" of the carbon-centered radical with the Fe(IV)-OH to form the hydroxylated product with high regioselectivity and stereo-retention.[43] Additionally, the prototype Fe-bTAML complex under homogeneous conditions displays poor turnover numbers for catalytic oxidation of hydrocarbons since it undergoes acid or base induced demetallation with chemical oxidants (e.g., mCPBA or NaOCl) (pH=12.6) (Figure S42). We need to i) modify the head part of the Fe-bTAML by introducing a $-NO_2$ group to increase its robustness to hydrolytic degradation,[44,45] and ii) use sodium phosphate buffer to maintain the pH of the reaction to achieve a high turnover number. In this case, high catalytic efficiency was observed with the prototype Fe-bTAML encapsulated inside the COF nano-spheres. Besides, no further use of base was required for maintaining the pH. The $[Fe^{III}(Cl)bTAML]^{2-}$@2X TpDPP COF nano-spheres could be recycled up to 4 cycles without altering the activity and selectivity of the catalyst (Figure 3d). The improved reactivity of $(Et_4N)_2[Fe^{III}(Cl)bTAML]$, when incarcerated inside the COF nano-spheres, resembles enzymes like cytochrome P450 in which the hydrophobic cavity facilitates oxidation of water-insoluble hydrophobic substrates by efficiently partitioning them inside the cavity. We wanted to explore if the oxidation of water-insoluble substrates could be carried out with $[Fe^{III}(Cl)bTAML]^{2-}$@2X TpDPP COF nano-spheres using water as the solvent. It should be noted that homogeneous C–H functionalization in water using Fe-complexes is an arduous task since the high-valent oxoiron intermediates formed upon addition of oxidant react with the O-H bond of water, which is present in much greater concentration. We have earlier shown the in 100% water, $(Et_4N)_2[Fe^{III}(Cl)bTAML]$ catalyzes water oxidation to form O_2 *via* the oxoiron(V) intermediate. However, our attempts for C–H functionalization were unsuccessful, as the COF nano-spheres aggregated in water.

Hence, we decided to construct TpDPP COF thin-films from the catalyst immobilized TpDPP COF nano-spheres *via* covalent self-assembly. Individual TpDPP COF nano-spheres undergo covalent self-assembly in the water-DCM bilayer or even while drop-casted on top of any support, and eventually form uniform COF nano-films. The COF nano-films are more crystalline and porous than COF nano-spheres and do not undergo any further transmutation in water. The covalent self-assembly driven by the free amine and

aldehyde functionality of the COF nano-spheres occurs *via* a unique, dynamic process previously unheard of. The attractive capillary forces and convective transport of the COF nano-spheres drive their self-assembly. Consequently, when two separate spheres come in contact, they start reacting *via a* reversible Schiff base reaction, which initiates the fibers/threads' protrusion at their interface (Figure 3a-i and section S-2). The distribution of fibers enhances with time to accomplish the formation of a COF nano-film of thicknesses of 250-270 nm after three days (Figure 5e-f and S44). It is quite fascinating that the probability/chance of immobilized $(Et_4N)_2[Fe^{III}(Cl)bTAML]$ molecules escaping from the COF nano-spheres to the bulk during the covalent self-assembly was nullified entirely by the non-covalent interactions of the catalyst molecules with the COF binding pockets. The dynamic transmutation from the nano-spheres ® nano-fibers ® nano-films did not affect the immobilized catalyst molecules and culminated in highly fecund catalytical COF thin-films. The EDX analysis confirmed uniform distribution of $(Et_4N)_2[Fe^{III}(Cl)bTAML]$ within COF nano-spheres, nano-films, and every intermediate phase during this transmutation process (Figure S37). We have monitored the spheres ® fibers ® film transmutation with confocal imaging to ascertain the immobilized catalysts' enduring stability during the covalent self-assembly (Figure 4j-m and section S-15). The confocal imaging revealed the uniform adsorption and distribution of (Rhodamine B) dye molecules inside the COF nano-spheres and COF fibers, which manifested their high porosity and adsorption capacity. These $(Et_4N)_2[Fe^{III}(Cl)bTAML]$ molecules are confined within the hydrophobic pockets of the COF thin-film. Because of the hydrophobicity of the $[Fe^{III}(Cl)bTAML]^{2-}$@TpDPP COF thin-films (contact angle 123.2°), only the hydrophobic substrates could contact the active catalytic sites but not the water molecules (Figure 5c and S41). The wt% loading of the $(Et_4N)_2[Fe^{III}(Cl)bTAML]$ catalyst within the COF nano-spheres and the COF thin-films were found to be 23 wt% and 19 wt%, respectively (Section S-7). The ICP-MS analysis of the catalyst immobilized COF nano-spheres and COF film showcased the percentage of metal (Fe) loading to be 4.5 and 3.6 wt% respectively.

We could achieve the heterogenous C–H functionalization in water for the very first-time using $(Et_4N)_2[Fe^{III}(Cl)bTAML]^{-}$ immobilized COF nano-films. To a dispersion of $[Fe^{III}(Cl)bTAML]^{2-}$@TpDPP COF thin-film in water was added adamantane and NaOCl (0.1 M, 250 eq. added iteratively), and the reaction was allowed to proceed for 1.5 hrs. Analysis of the products showed the formation of 1-adamantanol with 45% yield (47% conversion) and 141:1 (*3°*:*2°*) selectivity Figure 5a). With cis-dimethyl cyclohexane as the substrate, *cis* dimethyl cyclohexanol (yield 75%) was formed as the predominant product with 257:1 (3°:2°) regioselectivity and 155:1 (*cis:trans*) stereoretention from *cis*-dimethyl cyclohexane (Figure 5a). After the reaction, the $[Fe^{III}(Cl)bTAML]^{2-}$@TpDPP COF thin-film was recovered easily by centrifugation. The same thin-film was used for four more subsequent reactions, and the yield and selectivity were unchanged even after the fourth cycle (Figure 5d). We believe that the cis-dimethylcyclohexane preferentially partitions inside the COF nano-spheres in the COF film, and this allows the reaction of water-insoluble substrate oxidation in water. We could not achieve more than 65% conversion in each cycle, probably due to the substrate's similar binding affinity and the product inside the COF film in water. C–H bonds of other substrates such as *cis*-decahydroanthracene, ethylbenzene (EB), diphenylmethane (DPM), and ambroxide were also oxidized using the $[Fe^{III}(Cl)bTAML]^{2-}$@TpDPP

COF thin-film/NaOCl in water with high catalytic yield and excellent selectivity (Figure 5a-b and section S-19). Under optimized conditions, for *cis*-decahydroanthracene, *3°* hydroxylated products were obtained in 83% yield with 99% stereoretention without the formation of any *2°* hydroxylated products. Only keto products were found for the functionalization of EB, DPM, and ambroxide with 99% (acetophenone), 99% (benzophenone), and 91% (sclareolide) yields, respectively (Figure 5a-b and section S-19).

We performed a proof-of-concept flow catalysis[46,47] using catalyst immobilized COF thin-films on a macroporous solid polymeric support to establish the generality of this C–H functionalization approach (Figure 5g and section S-18,19). 90 mg (0.66 millimoles) adamantane was dissolved in 25 ml CH_3CN (0.66 millimoles of bromobenzene as internal standard). It was passed through ~5 mg of $[Fe^{III}(Cl)bTAML]^{2-}$@TpDPP COF thin-film (19wt% catalyst loading) for several cycles with iterative addition of NaOCl (0.06 M). After the 60^{th} cycle, this inflow catalysis showcased the 72% catalytic yield of 1-adamantanol with an excellent turnover number of 355±5 (Figure 5h).

Conclusion

In summary, we have designed and synthesized crystalline TpDPP COF nano-spheres and utilized their distinct morphology and dispersibility to create a bridge between homogeneous and heterogeneous catalysis. We have successfully immobilized an anionic macrocyclic catalyst, $[Fe^{III}(Cl)bTAML]^{2-}$, inside the porous COF nano-spheres, which was facilitated *via* N–H···O hydrogen bonding between the nano-spheres and the complex. We have conducted the functionalization of unactivated C-H bonds using the dispersed heterogeneous catalyst, resulting in increased conversion, yield, and a high degree of regio-selectivity. This stems from the ability of the cavity inside the nano-spheres to co-localize both the substrate and the catalyst in close proximity. We took advantage of the mesoscale "fiber protrusion" phenomenon of these porous nano-spheres and fabricated self-standing COF thin-films. We could arrest $(Et_4N)_2[Fe^{III}(Cl)bTAML]$ molecules during the nano-spheres ® thin-film transmutation. The cumulative effect of such intermolecular interactions prevented the immobilized catalyst molecules from being leached out of despite such dynamic transmutation. We have performed heterogeneous C–H functionalization in water for the first time with an enhanced degree of selectivity (*cis:trans* = 155:1, 3°:2°= 257:1 in case of *cis*-dimethylcyclohexane) using the catalyst immobilized COF thin-films. Further, we have showcased the inflow catalysis by fabricating the COF thin-film on a polymeric support. Since our predesigned COF nano-spheres and COF thin-films allowed the formation of the highly reactive transient oxoiron(V) intermediate in water, we believe that this strategy can be utilized to stabilize many other reactive and transient, synthetically useful catalytic intermediates for carrying out catalytic reactions in water.

Declarations

Data availability

All data supporting the findings of this study, including synthesis, experimental procedures, compound characterization, and GC-MS analyses are available within the Article and its Supplementary Information

Acknowledgment

HSS, SB acknowledges CSIR for Research fellowship. PM acknowledges IISER-Kolkata for the IPhD fellowship. R.B. acknowledges SwarnaJayanti Fellowship grant [DST/SJF/CSA-02/2016-2017], DST Mission Innovation [DST/TM/EWO/MI/CCUS/17 and DST/TMD(EWO)/IC5-2018/01(C)], DST SERB [CRG/2018/000314] for funding.

AUTHOR INFORMATION

Corresponding Author

r.banerjee@ncl.res.in

sayam.sengupta@iiserkol.ac.in

Contributions

R.B. and H.S.S. conceived and designed the project. H.S.S. and S.B. carried out most of the experimental works (contributed equally). S.S.G. and R.B. provided guidance. B.C. provided expertise with catalysis and GC-MS analysis. P.M. and H.K. helped in synthesis. H.S.S., S.B., B.C., S.S.G., and R.B. wrote the manuscript.

Additional information

Supplementary Information is available in the online version of the paper. Reprints and permissions information is available online at www.nature.com/reprints. Correspondence and requests for materials should be addressed to R. B.

ORCID

Rahul Banerjee: 0000-0002-3547-4746

Sayam Sen Gupta: 0000-0002-3729-1820

Himadri Sekhar Sasmal: 0000-0001-7355-8783

Saikat Bag: 0000-0002-0464-2276

Bittu Chandra: 0000-0001-6071-8071

Poulami Majumder: 0000-0003-3403-8931

Himangshu Kuiry: 0000-0002-7536-658X

Competing interests

The authors declare no competing financial interests.

References

1. Murai, S. et al. Efficient catalytic addition of aromatic carbon-hydrogen bonds to olefins. *Nature* **366,** 529-531 (1993).
2. Shilov, A. E. & Shul'pin, G. B. Activation of C-H bonds by metal complexes. *Rev.* **97,** 2879–2932 (1997).
3. Breslow, R., Huang, Y., Zhang, X. & Yang, J. An artificial cytochrome P450 that hydroxylates unactivated carbons with regio- and stereoselectivity and useful catalytic turnovers. *Natl. Acad. Sci.* **94,** 11156-11158 (1997).
4. Groves, J. T. & Neumann, R. Regioselective oxidation catalysis in synthetic phospholipid vesicles. Membrane-spanning steroidal metalloporphyrins. *Am. Chem. Soc.* **111,** 2900-2909 (1989).
5. Herrerias, C.I., Yao, X., Li, Z. & Li, C.J. Reactions of C−H Bonds in Water. *Rev.* **107,** 2546-2562 (2007).
6. Meunier, B., de Visser, S. P. & Shaik, S. Mechanism of oxidation reactions catalyzed by cytochrome P450 enzymes. *Rev.* **104,** 3947-3980 (2004).
7. Woggon, W.D. *Cytochrome P450: Significance, Reaction Mechanisms and Active Site Analogues;* Springer: Berlin Heidelberg, 1996.
8. Lewis, J.C., Coelho, P.S. & Arnold, F.H. Enzymatic functionalization of carbon–hydrogen bonds. *Soc. Rev.* **40,** 2003-2021 (2011).
9. Schmid, A. et al. Industrial biocatalysis today and tomorrow. *Nature* **409,** 258-268 (2001).
10. Breslow, R., Zhang, X. & Huang, Y. Selective Catalytic Hydroxylation of a Steroid by an Artificial Cytochrome P-450 Enzyme. *Am. Chem. Soc.* **119,** 4535-4536 (1997).
11. Narayan, S. et al. "On Water": Unique Reactivity of Organic Compounds in Aqueous Suspension. *Chem. Int. Ed.* **44,** 3275- 3279 (2005).
12. Fang, Z. & Breslow, R. A thiolate ligand on a cytochrome P-450 mimic permits the use of simple environmentally benign oxidants for biomimetic steroid hydroxylation in water. *Bioorganic & Medicinal Chemistry Letters* **15,** 5463–5466 (2005).
13. Santoro, S., Kozhushkov, S. I., Ackermann, L. & Vaccaro, L. Heterogeneous catalytic approaches in C–H activation reactions. *Green Chem.* **18,** 3471-3493 (2016).
14. Mack, J. B. C., Gipson, J. D., Bois, J. D. & Sigman, M. S. Ruthenium-Catalyzed C–H Hydroxylation in Aqueous Acid Enables Selective Functionalization of Amine Derivatives. *Am. Chem. Soc.* **139,** 9503–9506 (2017).
15. E. V. et al. An N-bridged high-valent diiron–oxo species on a porphyrin platform that can oxidize methane. *Nature Chemistry* **4,** 1024–1029 (2015).

16. Prat, D., Hayler, J. & Wells, A. A survey of solvent selection guides. *Green Chem.* **16,** 4546-4551 (2014).
17. According to the ACS Green Chemistry Institute Pharmaceutical Roundtable (GCI-PR) guide, water is the most sustainable and recommended solvent for any chemical reaction
18. Côte, A. P. et al. Crystalline, Covalent Organic Frameworks. *Science* **310,** 1166–1170. (2005).
19. Gropp, C., Ma, T., Hanikel, N. & Yaghi, O. M. Design of higher valency in covalent organic frameworks. *Science* **370,** 424-431 (2020).
20. Xu, H., Gao, J. & Jiang. D. Stable, crystalline, porous, covalent organic frameworks as a platform for chiral organocatalysts. *Chem.* **7,** 905–912 (2015).
21. Li, X. et al. Squaramide-Decorated Covalent Organic Framework as a New Platform for Biomimetic Hydrogen-Bonding Organocatalysis *Commun*. **55,** 5423-5426 (2019).
22. Han, X. et al. Chiral Covalent Organic Frameworks with High Chemical Stability for Heterogeneous Asymmetric Catalysis. *Am. Chem. Soc.* **139,** 8693–8697 (2017).
23. Piermatti, O., Abu-Reziq, R. & Vaccaro, L. *Strategies to Immobilized Catalysts: A Key Tool for Modern Chemistry. In Catalyst Immobilization;* Wiley-VCH Verlag GmbH & Co. KGaA: Weinheim, Germany, 2020.
24. Ye, R., Zhao, J., Wickemeyer, B. B., Toste, F. D. & Somorjai, G. A. Foundations, and strategies of the construction of hybrid catalysts for optimized performances. *Nature Catalysis* **1,** 318–325 (2018).
25. Gottschling, K. et al. Rational Design of Covalent Cobaloxime–Covalent Organic Framework Hybrids for Enhanced Photocatalytic Hydrogen Evolution. *Am. Chem. Soc.* **142,** 12146–12156 (2020).
26. Collins, T.J. & Ryabov, A.D. Targeting of high-valent Iron-TAML activators at hydrocarbons and beyond. *Rev.* **117,** 9140–9162 (2017).
27. Ghosh, M.et al. Formation of a Room Temperature Stable FeV(O) Complex: Reactivity Toward Unactivated C–H Bonds. *Am. Chem. Soc.* **136,** 9524 (2014).
28. Sasmal, H.S. et al. Covalent Self-Assembly in Two Dimensions: Connecting Covalent Organic Framework nanospheres into crystalline and porous thin-films. *Am. Chem. Soc.* **141,** 20371–20379 (2019).
29. Diercks, C. S. & Yaghi, O. M. The atom, the molecule, and the covalent organic framework. *Science* **355,** 923 (2017).
30. Kandambeth, S. et al. Construction of crystalline 2D Covalent Organic Frameworks with remarkable chemical (Acid/Base) stability via a combined reversible and Irreversible route. *Am. Chem. Soc.* **134,** 19524–19527 (2012).
31. Mow, R. E. et al. Colloidal Three-Dimensional Covalent Organic Frameworks and their application as porous liquids. *Mater. Chem. A* **8,** 23455-23462 (2020).
32. DeBlase, C. R., Silberstein, K. E., Truong, T. T., Abruna, H. D. & Dichtel, W. R. β-Ketoenamine-Linked Covalent Organic Frameworks capable of pseudocapacitive energy storage. *Am. Chem. Soc.* **135,** 16821–16824 (2013).

33. de Visser, P.S. Second-coordination sphere effects on selectivity and specificity of heme and nonheme iron enzymes. *Eur.J.* **26,** 5308 –5327 (2020).
34. S. et al. A Manganese(V)−Oxo Complex: Synthesis by Dioxygen Activation and Enhancement of Its Oxidizing Power by Binding Scandium Ion. *J. Am. Chem. Soc.* **138,** 8523-8532 (2016).
35. Ottenbacher, R. V., Talsi, E. P. & Bryliakov, K. P. Mechanism of Selective C−H Hydroxylation Mediated by Manganese Aminopyridine Enzyme Models. *ACS Catal.* **5,** 39–44 (2015).
36. Triggs, N.E. & Valentini, J.J. An investigation of hydrogen bonding in amides using Raman spectroscopy. *Phys. Chem.* **96,** 6922–6931 (1992).
37. Xue, S. et al. Enhanced redox reactivity of a nonheme iron(V)−oxo complex binding proton. *Am. Chem. Soc.* **142,** 15305–15319 (2020).
38. Zhou, S. et al. Hydrogen bonding interaction of poly(D,L-Lactide)/hydroxyapatite nanocomposites. *Mater.* **19,** 247–253 (2007).
39. Karak, S. et al. Constructing ultraporous Covalent Organic Frameworks in seconds via an organic terracotta process. *Am. Chem. Soc.* **139,** 1856−1862 (2017).
40. Chandra, B., Helllan, K. M., Pattanayak, S. and Gupta, S. S. Oxoiron(V) mediated selective electrochemical oxygenation of unactivated C-H and C=C bonds using water as oxygen source. *Sci.* **11,** 11877-11885 (2020).
41. Chandra, B., De, P. & Gupta, S.S. Selective oxygenation of unactivated C-H bonds by dioxygen via an autocatalytic formation of oxoiron(V) species. *Commun.* **56,** 8484-8487 (2020).
42. Qiu, Y. & Hartwig, J.F. Mechanism of Ni-Catalyzed Oxidations of Unactivated C(sp^3)−H Bonds. *Am. Chem. Soc.* **142,** 19239-19248 (2020).
43. Huang, X. & Groves, J.T. Beyond ferryl-mediated hydroxylation: 40 years of the rebound mechanism and C−H activation. *JBIC Journal of Biological Inorganic Chemistry* **22,** 185-207 (2017).
44. Ghosh, M. et al. Selective C-H bond oxidation catalyzed by Fe-bTAML complex: Mechanistic implications. *Inorg. Chem.* **56,** 10852-10860 (2017).
45. Jana, S., Ghosh, M., Ambule, M. & Gupta, S.S. Iron complex catalyzed selective C-H Bond oxidation with broad substrate scope. *Lett.* **19,** 746-749 (2017).
46. Shore, G., Morin, S. & Organ, M. G. Catalysis in Capillaries by Pd Thin-films Using Microwave-Assisted Continuous-Flow Organic Synthesis (MACOS). *Chem. Int. Ed.* **45,** 2761-2766 (2006)
47. Yang, C. et al. Heterogeneous photoredox flow chemistry for the scalable organosynthesis of fine chemicals. *Commun.* ***11,***1239-1246 (2010).

Figures

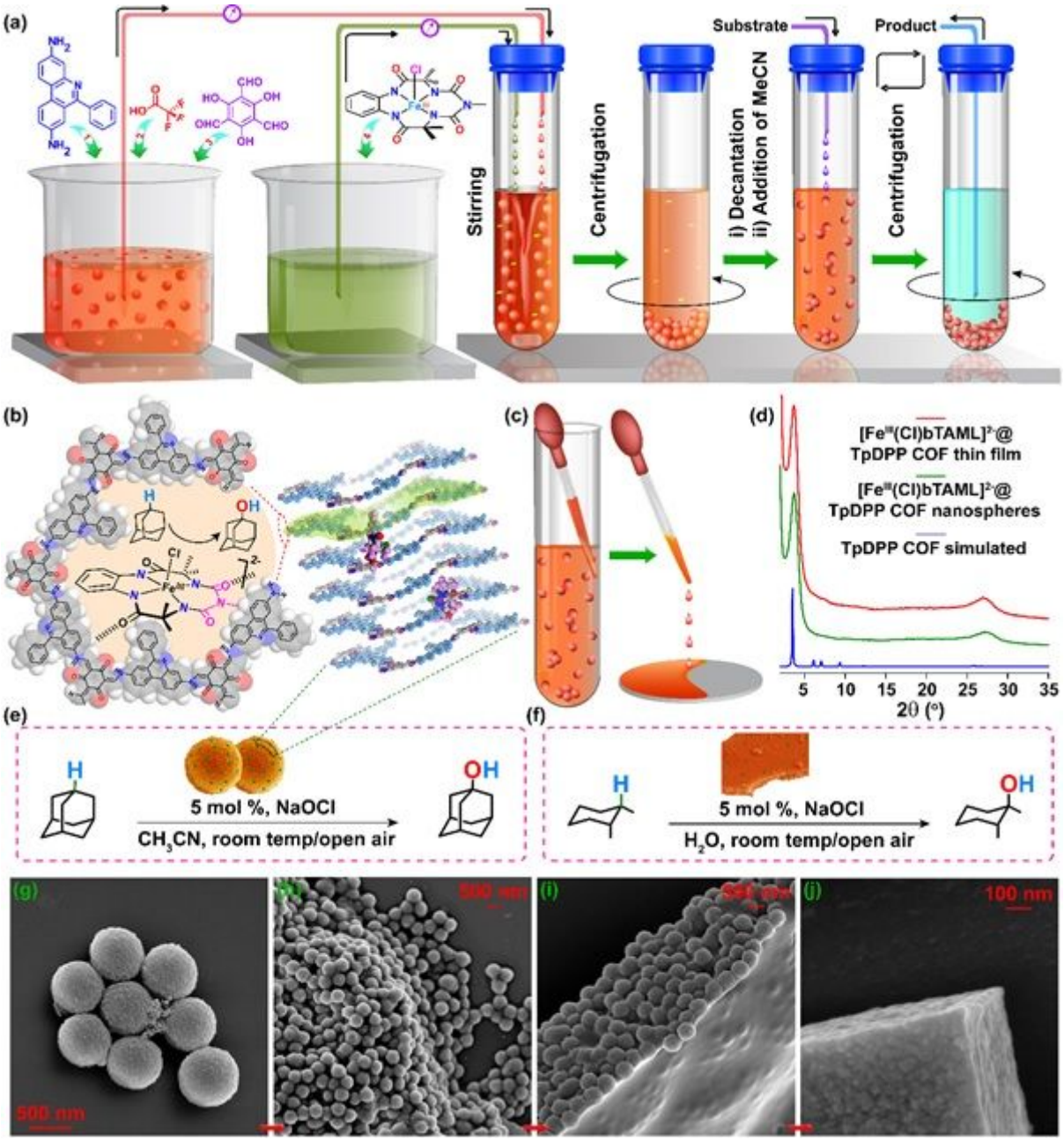

Figure 1

A general strategy for design and construction of catalytic COF nano-spheres and COF thin-films. (a) Schematic representation of the synthesis of the crystalline, porous TpDPP COF nano-spheres and the immobilization of the (Et4N)2[FeIII(Cl)bTAML] catalyst within the TpDPP COF nano-spheres. (b) Schematic representation of the catalytic reaction within the pockets (the ordered pores) of the TpDPP COF nano-spheres' crystallites. (c) Fabrication of the TpDPP COF thin-film from catalyst immobilized TpDPP COF nano-spheres (via multiple drop-casting mediated covalent self-assembly). (d) Experimental PXRD pattern of [FeIII(Cl)bTAML]2-@TpDPP COF nano-spheres and [FeIII(Cl)bTAML]2-@TpDPP COF thin-film. (e-f) The C–H hydroxylation was performed using the catalytic COF nano-spheres in acetonitrile and catalytic COF thin-film in water. (g-j) The sequence of transformation from catalytic COF nano-spheres to

catalytic COF thin-film (via covalent self-assembly at the DCM-water interface) is demonstrated via SEM imaging.

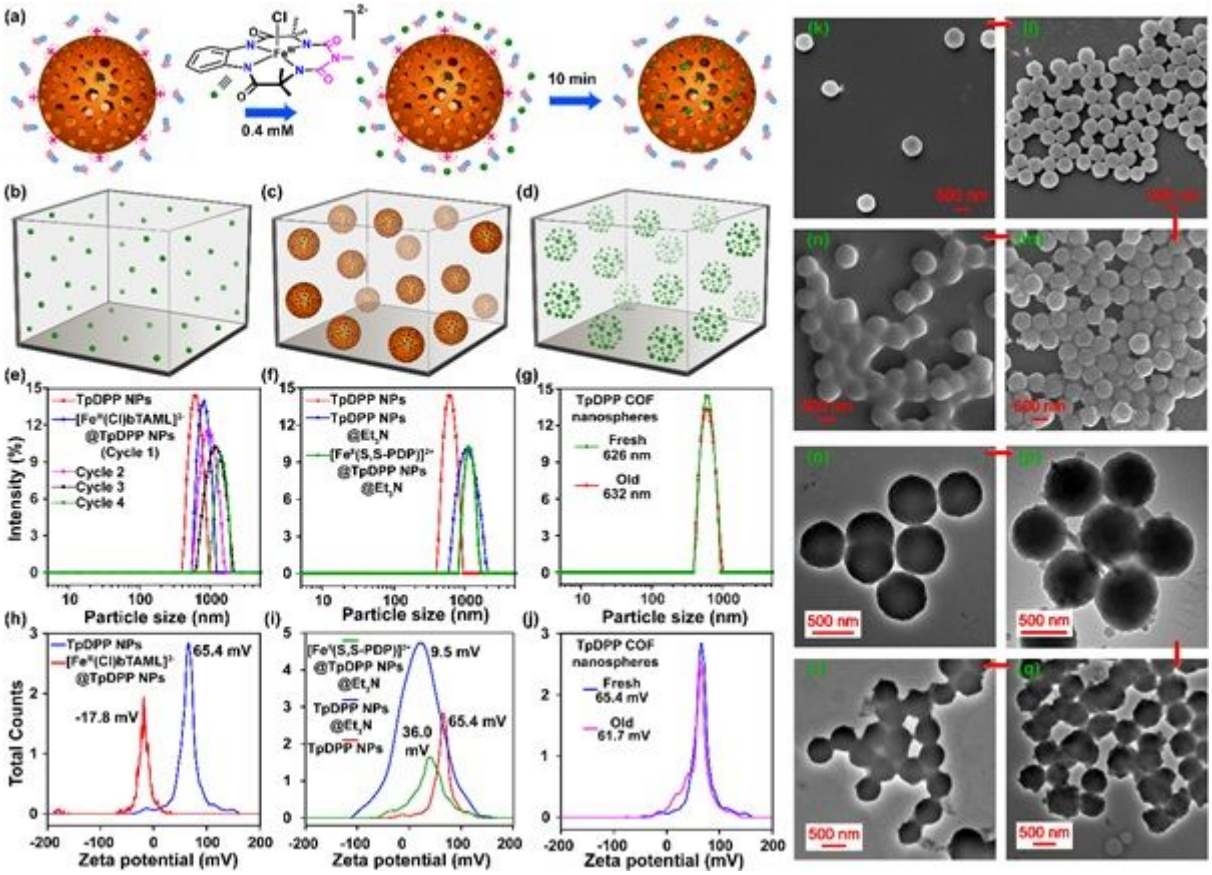

Figure 2

Selective immobilization of catalysts within porous COF nano-spheres. (a) Schematic representation of the adsorption of (Et4N)2[FeIII(Cl)bTAML] solution in acetonitrile by TpDPP COF nano-spheres. (b-d) Spatial confinement of the active catalytic sites within the condensed space of COF nano-spheres. (e) The changes in the size of the (Et4N)2[FeIII(Cl)bTAML] catalyst embedded nano-spheres after each cycle of catalysis measured by the DLS analyses. (f) The changes in the size of the COF nano-spheres after treating with Et3N and consequent immobilization of the [FeII(S, S-PDP)](SbF6)2 catalyst. (g) The stability of the as-synthesized COF nano-spheres in solution concerning their sizes after four months. (h) Zeta potential of the as-synthesized COF nano-sphere and after the immobilization of the anionic macrocyclic (Et4N)2[FeIII(Cl)bTAML] catalyst within the COF nano-spheres. (i) Zeta potential of the as-synthesized COF nano-spheres, neutralized COF nano-spheres and after the immobilization of the [FeII(S, S-PDP)](SbF6)2 catalyst within neutralized COF nano-spheres. (j) The stability of the as-synthesized COF nano-spheres in solution concerning their zeta potential after four months. (h) The electrokinetic potential of the as-synthesized COF nano-spheres after four months. (k-n) SEM and (o-r) TEM images of the catalytic COF nano-spheres used for the 1st, 2nd, 3rd, and 4th cycles of the catalytic reaction (recyclability of the catalytic COF nano-spheres), respectively.

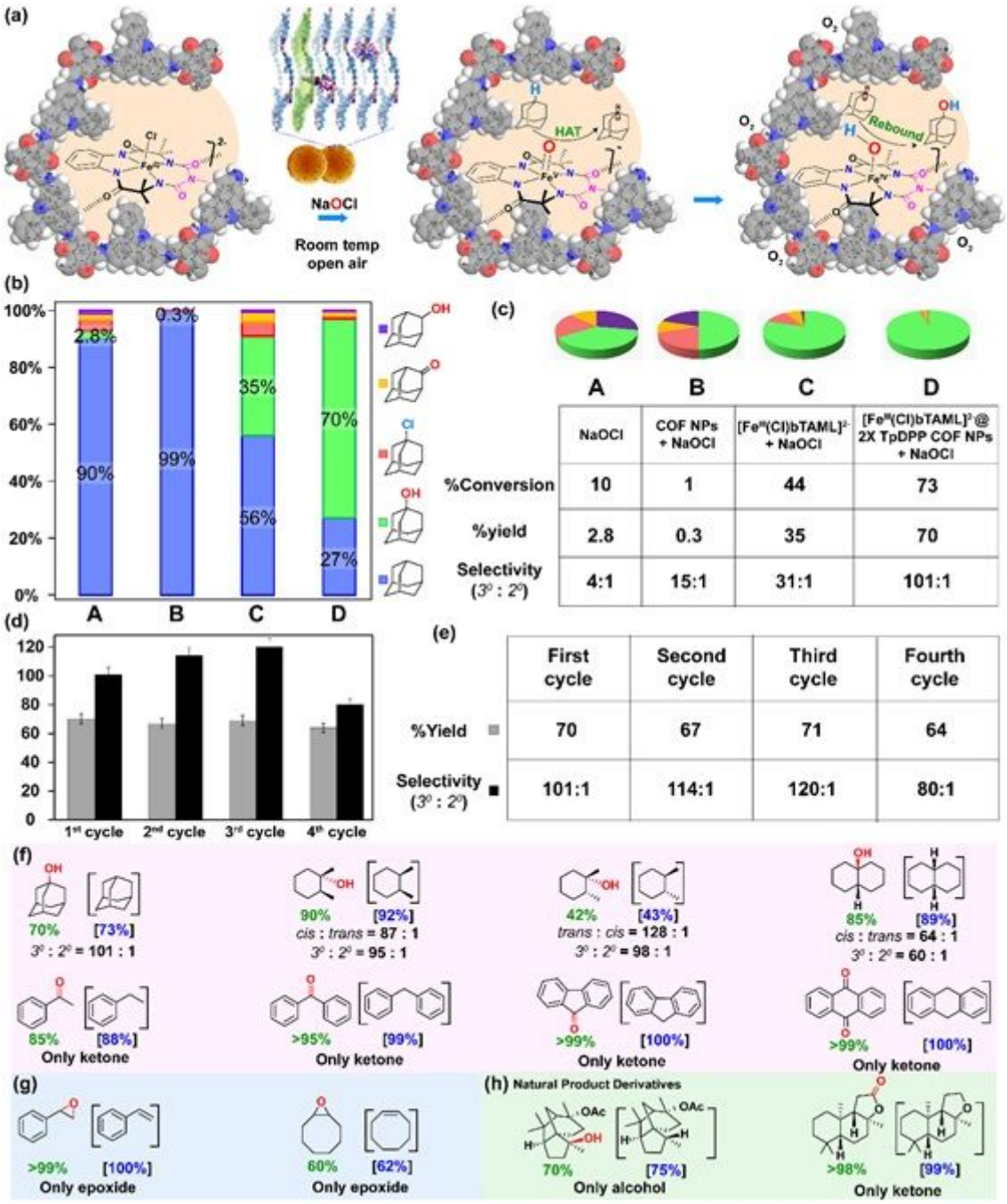

	NaOCl	COF NPs + NaOCl	$[Fe^{III}(Cl)bTAML]^{2-}$ + NaOCl	$[Fe^{III}(Cl)bTAML]^{2-}$ @ 2X TpDPP COF NPs + NaOCl
%Conversion	10	1	44	73
%yield	2.8	0.3	35	70
Selectivity ($3^{\circ} : 2^{\circ}$)	4:1	15:1	31:1	101:1

	First cycle	Second cycle	Third cycle	Fourth cycle
%Yield	70	67	71	64
Selectivity ($3^{\circ} : 2^{\circ}$)	101:1	114:1	120:1	80:1

Figure 3

egio and Stereoselective C—H functionalization by catalytic COF nano-spheres in acetonitrile. (a) Schematic representation of the plausible mechanism for heterogeneous catalysis and catalytic pathway. (b-c) Yield and selectivity of 1-adamantanol in different reaction conditions (homogeneous and heterogeneous) and some control experiments. (d-e) The recyclability of the catalyst up to four cycles. Error bars denote the standard error (standard deviation of the mean). (f-h) Substrate scope for the heterogeneous C-H functionalization in acetonitrile.

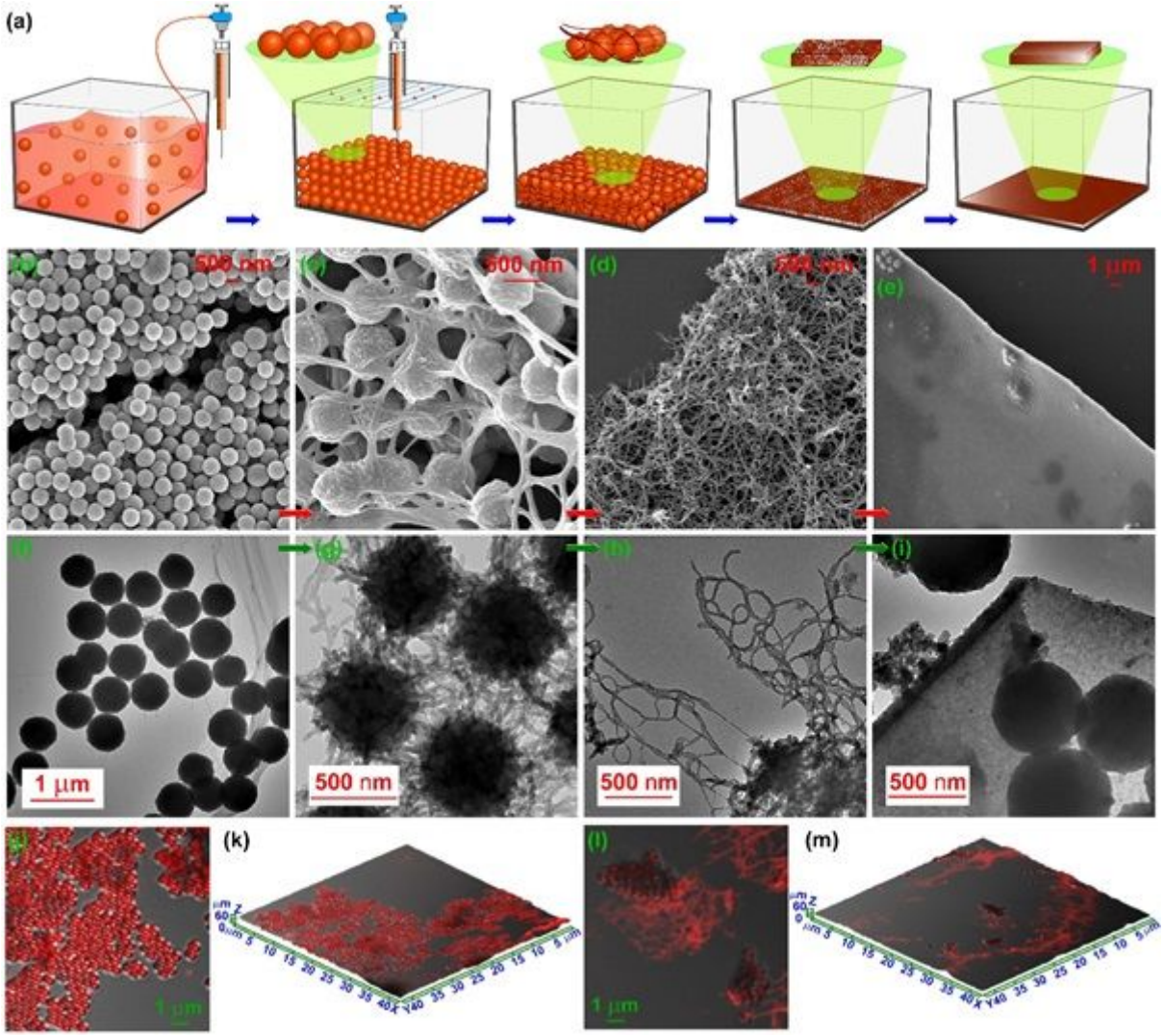

Figure 4

Mechanism of the transmutation from COF nano-spheres to nano-films. (a) Schematic representation of catalytic COF thin-films' fabrication from catalyst embedded COF nano-spheres via covalent self-assembly. The generation of COF threads at the two COF nano-spheres' interface during this unique covalent self-assembly should be noted. (b-e) SEM and (f-i) TEM imaging revealing the mechanism of the transmutation of the catalytic COF nano-spheres -> fibers -> thin-films. (j-m) The confocal imaging of the transmutation mechanism by adsorption of Rhodamine B dye.

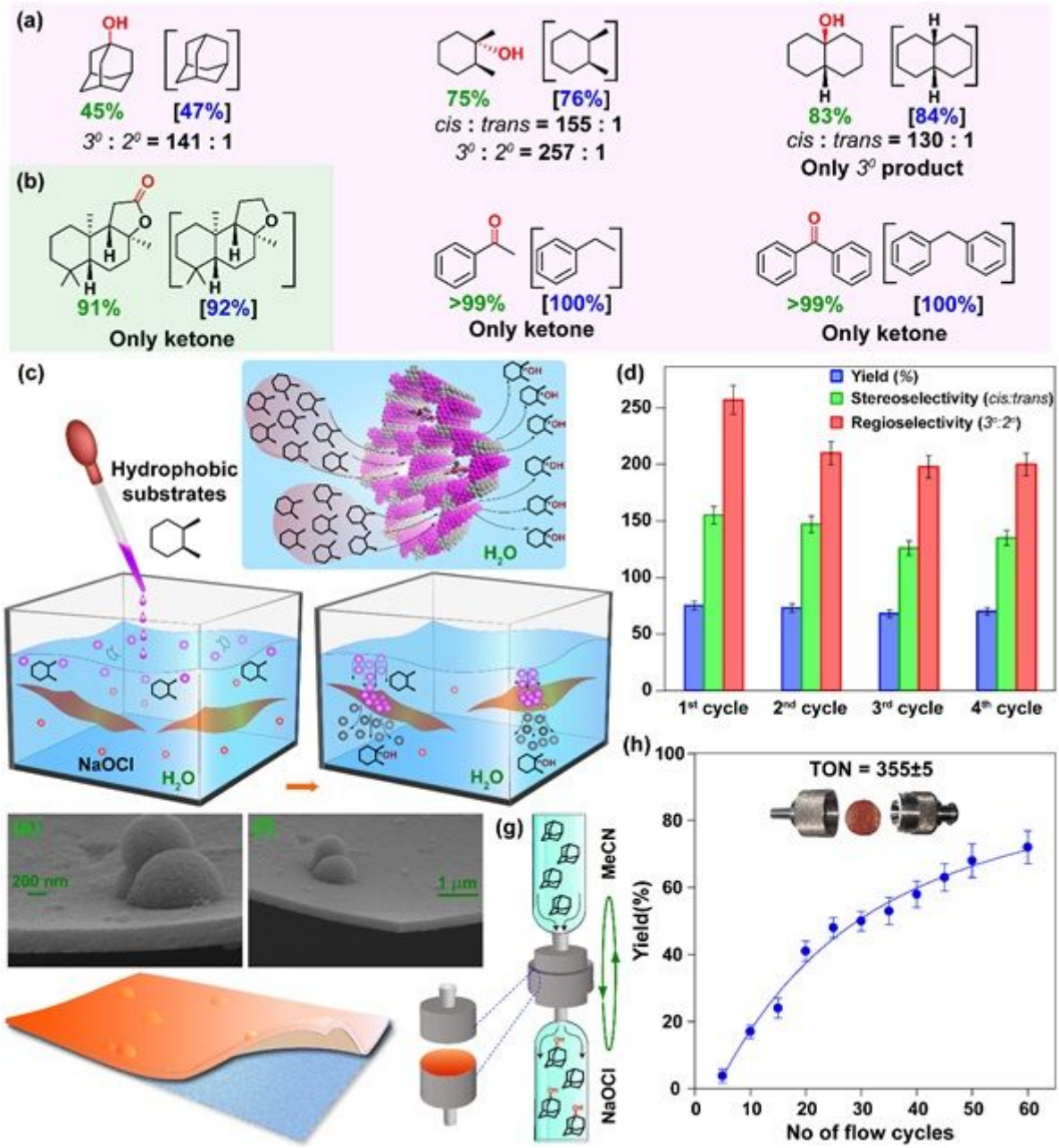

Figure 5

Regio and Stereoselective C–H functionalization by catalytic COF nano-films in water. (a-b) The substrate scope of the heterogeneous C-H functionalization in water using catalytic TpDPP COF thin-film. (c) Schematic representation of the catalytic process of the functionalization of hydrophobic substrates by catalytic COF thin-film in water. (d) Recyclability of the catalytic COF thin-film for heterogeneous C-H functionalization of cis-dimethyl cyclohexane in water. Error bars denote the standard error. (e) Schematic representation of the catalysis inflow using catalyst immobilized COF thin-films fabricated on a macroporous solid polymeric support. (f-g) SEM images of the catalytic thin-film having a thickness of 250-270 nm. (h) The catalytic yield of 1-adamantanol concerning the number of flow cycles. Error bars denote the standard error.

Supplementary Files

This is a list of supplementary files associated with this preprint. Click to download.

- SubmitESINatureChemistry07012021.pdf
- TableofContentsGraphic.jpg